Read noise for a 2.5µm cutoff Teledyne H2RG at 1-1000Hz frame rates

Roger M. Smith[1], David Hale
California Institute of Technology, 1200 East California Blvd, Pasadena CA 91125, USA

ABSTRACT

A camera operating a Teledyne H2RG in H and Ks bands is under construction at Caltech to serve as a near-infrared tip-tilt sensor for the Keck-1 Laser Guide Star Adaptive Optics system. After imaging the full field for acquisition, small readout windows are placed around one or more natural guide stars anywhere in the AO corrected field of view. Windowed data may be streamed to RAM in the host for a limited time then written to disk as a single file, analogous to a "film strip", or be transmitted indefinitely via a second fiber optic output to a dedicated computer providing real time control of the AO system. The various windows can be visited at differing cadences, depending on signal levels. We describe a readout algorithm that maximizes exposure duty cycle, minimizes latency, and achieves very low noise by resetting infrequently then synthesizing exposures from Sample Up The Ramp data. To illustrate which noise sources dominate under various conditions, noise measurements are presented as a function of synthesized frame rate and window sizes for a range of detector temperatures. The consequences of spatial variation in noise properties, and dependence on frame rate and temperature are discussed, together with probable causes of statistical outliers.

Keywords: H2RG, read noise, wavefront sensor, NIR, frame rate, noise map, multiplexor glow, Random Telegraph Noise

1. INTRODUCTION

After a brief introduction to the instrument, this paper focuses on the relationship between frame rate and readout noise as a function of region of interest (ROI) size and temperature. The shapes of these curves will be traced to a variety of familiar noise mechanisms, and some optimizations will be discussed. The most unusual findings are that noise at low frame rates can be dominated by multiplexor glow, and that the bad pixel map is dominated by Random Telegraph Noise rather than sensitivity drop outs or hot pixels. This results in a bad pixel map, which is highly dependent on frame rate as well as temperature.

The Keck-1 adaptive optics system, which feeds the NIR integral-field spectrograph, OSIRIS, employs a sodium laser to provide a beacon for high order wavefront sensing at any telescope pointing. The light from the laser follows the same path on its outward and return journeys, making it insensitive to wavefront tilt, so the centroid of a natural guide star must be measured to provide feedback to the tip-tilt mirror, which compensates for image motion. Previously the Keck-1 AO system used an optical camera to sense tip-tilt, but an infrared guide star sensor, operating in Ks or H band, is preferred since it benefits from the higher Strehl delivered by the AO system at longer wavelengths. These higher Strehl ratios translate to greater sensitivity (better contrast against sky) and better centroiding accuracy, which scales as signal-to-noise ratio (S/N) divided by full-width at half maximum (FWHM). In addition, NIR guide stars are available in fields that are obscured by dust in the optical. The net result is a significant increase in sky coverage and/or delivered image quality, as shown in Figure 1.

The light from the guide star is diverted to the NIR tip-tilt sensor (also known as TRICK) by a dichroic (e.g. selecting H band light from a science target observed in K band) or by an annular mirror, which picks off one or more stars surrounding the science field. An ideal wavefront sensor will be able to select stars from anywhere in the field of view of the adaptive optics system to provide images of one or several guide stars at rates up to a kilohertz, with noise which is insignificant compared to the shot noise required to obtain sufficient centroiding accuracy. In practice this means that 3 electron read noise is highly desirable, with marginal gains if noise can be reduced further. When guide stars of sufficient brightness are not available, some servo loop bandwidth can be sacrificed to allow longer exposure times (lower frame rates) which provide the double benefit of increasing the integrated signal and allowing more time for noise reduction through averaging of non-destructive readouts, a key feature of the hybrid-CMOS image sensor.

[1] rsmith@astro.caltech.edu, Phone 1 (626)-395-8780

High Energy, Optical, and Infrared Detectors for Astronomy V, edited by Andrew D. Holland, James W. Beletic,
Proc. of SPIE Vol. 8453, 84530Y · © 2012 SPIE · CCC code: 0277-786X/12/$18 · doi: 10.1117/12.927148

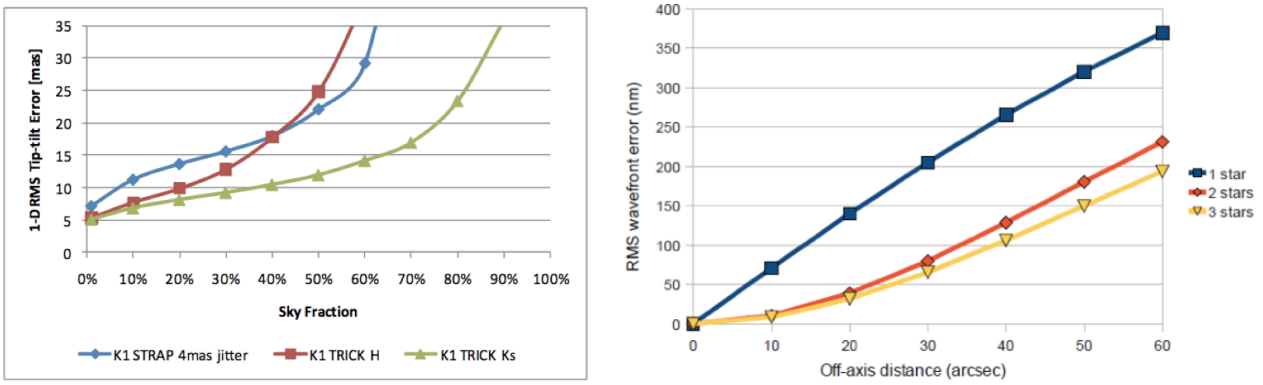

Figure 1: Left: Strehl for K band science target with on axis M0 guide star measured in Ks or H bands wth TRICK (4x4 pixels, 50mas/pixel) or R band with STRAP (2x2 pixels at 900mas/pix). Right: wavefront errors for Mauna Kea turbulence profile and 10m primary mirrors and two stars at 180 degrees or three at 120 degrees.

2. THE TRICK CAMERA

The full 120 arc-minute field of view of the Keck-1 AO system is reimaged onto a 2.5µm cut-off Teledyne HAWAII-2RG (H2RG) NIR sensor at 50 milliarcseconds per pixel as shown in Figure 2. The use of a large sensor and full field reimaging not only eliminates the need for guide probes, but also provides very accurate positioning of multiple guide stars at little extra cost. When using off axis guide stars, having several which surround the science field allows interpolation to correct for wavefront tilt variation across the field, while also improving the S/N on the basic tilt measurement.

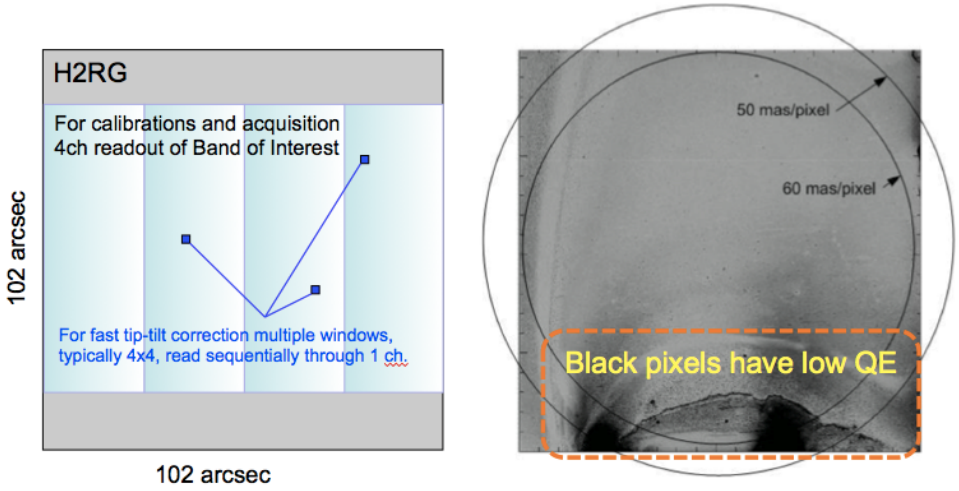

Figure 2. At 50 milliarcseconds per pixel, the 120 arcminute field of view (depicted at right) passes slightly outside the edges, but slightly inside the corners, of the 2044x2044 pixel image area of the H2RG.

Two BaF_2 field lenses at ambient temperature lie slightly ahead of the AO system's output focal plane. A gold mirror folds the horizontal beam upwards through a downward-looking dewar window. This is tilted to compensate for astigmatism introduced when the AO system corrects for astigmatism in the science beam caused by the dichroic. The remainder of the optics is cold and well baffled to prevent thermal radiation outside the beam from reaching the detector. Pupil stops are machined into the filter wheel such that the H band pupil is oversized for maximum throughput while the K band pupil stop is inscribed within the image of the ragged edge of the hexagonally tiled primary mirror.

A Joule-Thomson refrigerator with non-flammable refrigerant from Advanced Research Systems, Inc. cools the system so that the first optic and filter wheel reaches 100K. The detector, which sits atop the relatively low conductivity invar lens tower, will be thermally regulated to 110K. The noise curves presented below were studied as a function of

temperature in a separate test dewar to determine what refrigeration options would be acceptable. The exploration of noise performance at higher temperatures was originally motivated by the lack of a low temperature refrigerant option for the Polycold Compact Cooler[1] that was free of flammable components. By changing to the "Orsa" Joule Thomson cooler[2] made by Advanced Research Systems, a much lower final cold head temperature was achieved using a non-flammable refrigerant (MR-90) at the cost of increasing the dewar length by several inches to accommodate the longer cold head assembly. The lower temperature provides greater margin for detector dark current and less stringent requirements for low thermal resistances in mechanical joints. The choice of the Orsa cooler was also strongly influenced by the MR-90 refrigerant's flat power curve that avoids the thermal slew rate peak induced by the cooling power spike seen in the Polycold power-temperature curves.

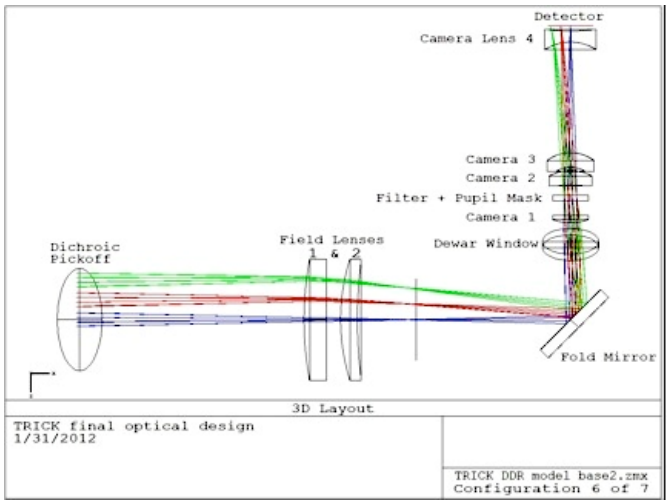

Figure 3. Optical layout. Warm field lenses 1 & 2 and (cold) camera lenses 1 & 2 are BaF_2, while the tilted window and camera lenses 3 & 4 are made from Infrasil.

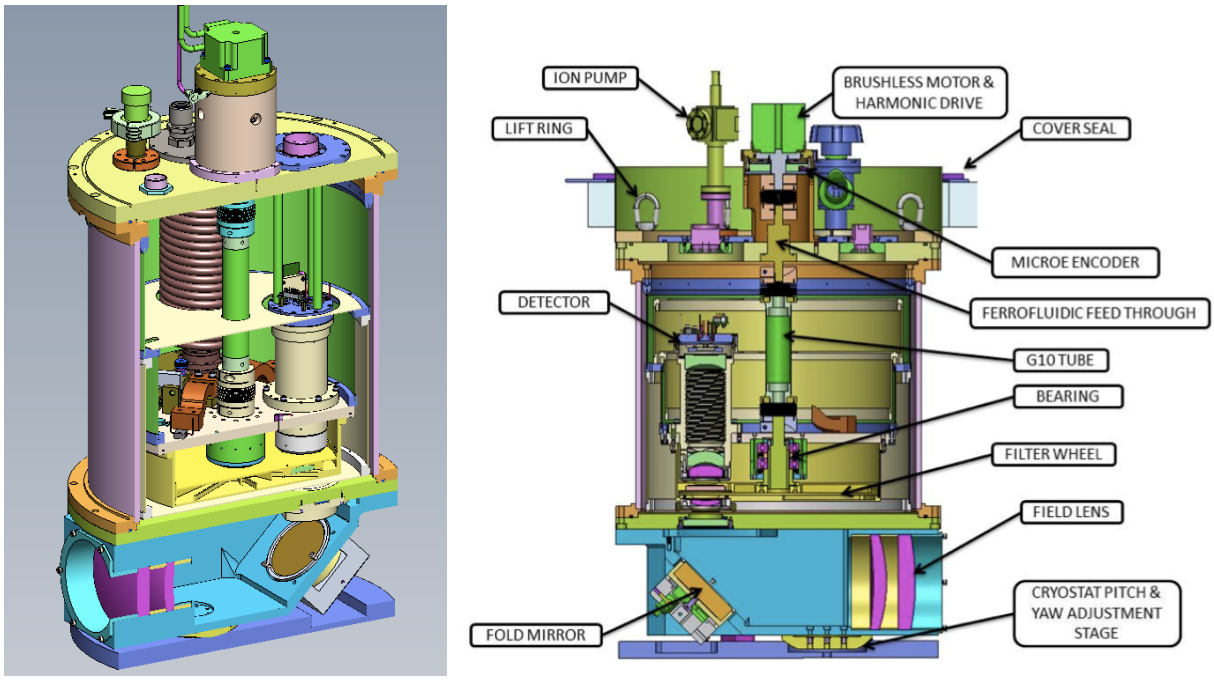

Figure 4. Cross-sectional views of the TRICK dewar. The cyan colored base and contents are at room temperature.

2.1 Controller layout and protocols.

The camera utilizes a little known option in the Astronomical Research Cameras Inc. controller. A second Hotlink fiber output is supplied on the "ARC-22" gen-3 timing board. This was intended by the designers to double the data rate to the host but we have used it to route a continuous stream of raw data to an alternative location, the Real Time Controller (RTC) within the Adaptive Optics system as shown in Figure 5. We further modified the ARC-22 timing board to enable writing of custom data words to the second fiber transmitter, for the purpose of creating a data header that can identify packets and flag configuration changes in the pixel stream to the RTC.

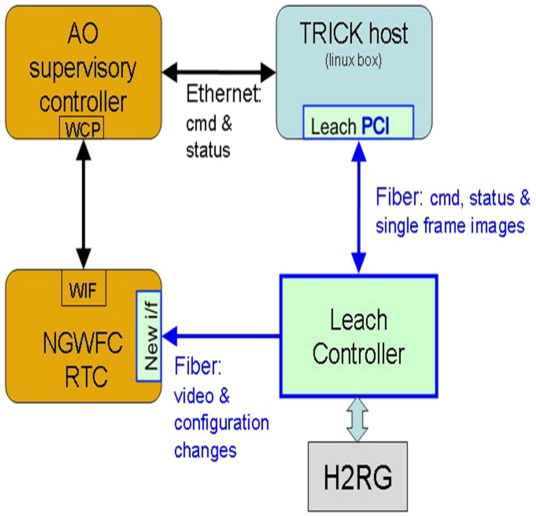

Figure 5. Controller layout. The second "Hotlink" optical fiber output on the ARC-22 timing board within the detector controller provides a direct 250 Mbit/s data path to the Real Time Controller in the Adaptive Optics system.

Pixel data are normally transferred directly from the AD converters to the fiber transducer without passing through the Digital Signal Processor on the timing board. The readout configuration (a list of window positions, sizes and visitation cadences) is transmitted to the RTC each time a reset occurs. The configuration is embedded in the data stream, rather than being sent to the RTC independently, to avoid command race conditions.

3. READOUT

3.1 Readout modes

The TRICK software supports conventional single frame correlated double sampled readout of the full frame or a single Band of Interest, reading out through multiple channels. (While the software and controller wiring support all H2RG output modes (1, 4, or 32 outputs) only one 8 channel video card is currently installed restricting readout to four channels.) This conventional readout mode sends the raw data to the TRICK Host computer, and is used for general detector testing and calibration. It will only be used for field acquisition in dust-obscured fields, since CDS readout through four channels will take 13 seconds and a faster optical imaging camera is available.

Multiple regions of interest are supported, reading in window mode through a single channel, with raw data normally flowing to the RTC via the second fiber link. The row and column pointers are set to the start address when a frame start pulse is received so that it is not necessary to clock from the corner of the array. Both start and end coordinates are used by the global reset logic to reset only the pixels within the window. Writing to registers in the multiplexor sets new window coordinates over the serial control link. All four parameters can be updated in 10 µs.

Table 1 shows the parameters that define a multi-window readout. Any line(s) in the table can be modified without interrupting the readout. Changes are queued up until they take effect at the next reset, typically every second or less. The new configuration is transmitted to the RTC at each Reset. Window readout cadences can differ, with the time between visits being moderately uniform. This is implemented by reading a window each time the loop counter is divisible by its "periodicity" parameter in the configuration table. e.g. If Periodicity=1, the window is visited every time

the loop is executed, or if Periodicity=N it is visited every Nth time around the loop. A delay may be inserted after each window is read to extend the exposure time per sample.

For testing the windowed readout described above, a capability is provided to stream a fixed number of frames of data to the host where it is buffered in memory and then written to disk as a single FITS file in which the raw frames have been concatenated along columns, with the later frames occupying the higher frame numbers. Due to the obvious analogy, we refer to this as a filmstrip. 512MB of RAM will support full speed acquisition for 1500s.

Table 1. Configuration table for readout of multiple windows at different cadences (3 windows in this example).

Periodicity	Delay	Start Col	Start Row	# Columns	# Rows
P1	T1	X1	Y1	ΔX1	ΔY1
P2	T2	X2	Y2	ΔX2	ΔY2
P3	T3	X3	Y3	ΔX3	ΔY3

3.2 Differential Multi-Accumulate

In the Fowler Sampling algorithm commonly used to improve read noise (Figure 6), the time spent resetting then averaging samples at the start of the exposure is effectively dead time since photons are either not collected during reset or are ignored if they arrive prior to a sample.

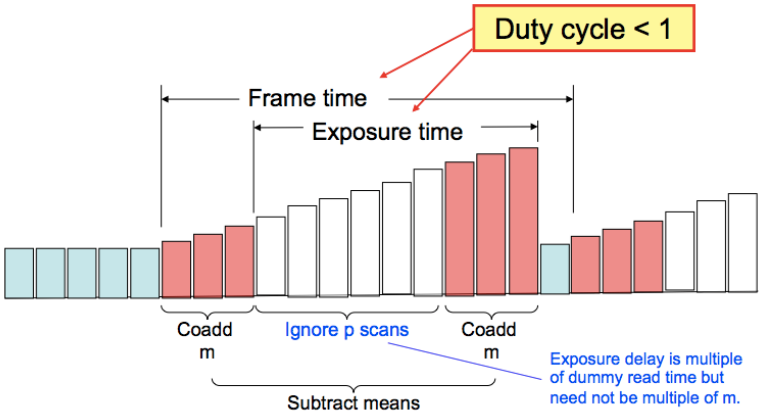

Figure 6. Fowler sampling: each rectangle represents frame scans with time on the horizontal axis and signal on the vertical axis. The average of the initial samples is subtracted from the average of final values. The time spent resetting and establishing the post-reset pixel value results in an effective exposure time loss so it is necessary to balance the improvement in read noise against the loss of signal photons.

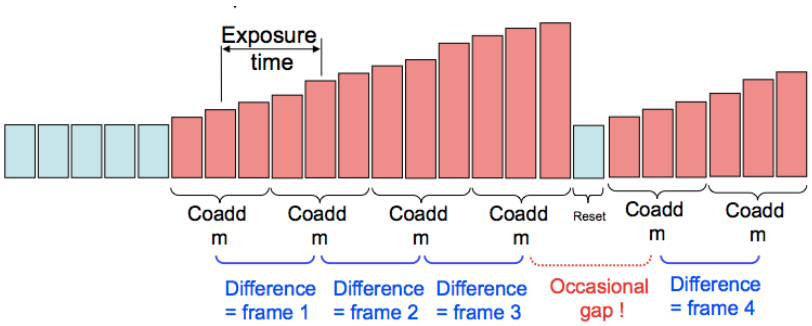

Figure 7. Differential Multi-Accumulate readout: continuous non-destructive readout is employed, resetting the windows only when the integrated signal approaches the pixel capacity. Groups of samples are coadded and then subtracted to synthesize the frame rate desired with minimal noise.

The Differential Multi-Accumulate readout employs continuous sampling (up the ramp) with sample averaging in groups (as for JWST's "Multi-Accumulate" readout). Successive averages are differenced to synthesize the Fowler sampled exposures. Since the samples averaged at the end of one exposure serve as the baseline for the next exposure there is no overhead to establish the initial level and no photons are ignored.

The exposure duty cycle is nearly 100%, with the only overhead being the time to perform a global reset and read the initial sample group. Many sample groups can be acquired before resetting since guide stars are seldom bright enough to use up an appreciable fraction of the pixel capacity in a single exposure. In the rare case that a signal is so bright that resets become frequent, then the signal to noise ratio will be high enough that a loss of duty cycle will be of little concern. For a single 4x4 window, the minimum time between resets is 250 µs (2 frame scans), but typical times will be tenths to a few seconds (hundreds to thousands of frames)

4. NOISE PERFORMANCE

All curves in this paper showing noise versus frame rate were obtained in single window mode reading at full speed for a variety of window sizes. The pixels were streamed to the host computer's RAM and written as filmstrip files in FITS format. As all the noise data were taken in the dark, resets only occurred before and after the filmstrip. The various frame rates shown on the plots were synthesized by reprocessing the raw data recorded in the filmstrips. A new filmstrip file was obtained when other parameters like window size or temperature were altered. All detectors tested were the "low noise ground based astronomy" recipe, H2RG-220 or TRICK's H2RG-222, operated with the bias voltages shown in Table 2.

Table 2. H2RG operating parameters.

Detector serial number	#220	#222
VDD	3.3V	3.3V
VDDA	3.3V	3.3V
BIASPOWER	3.3V	3.3V
BIASGATE	2.33V	2.33V
VRESET	0.3V	0.3V
DSUB	0.5V	0.475V

4.1 Pixel timing

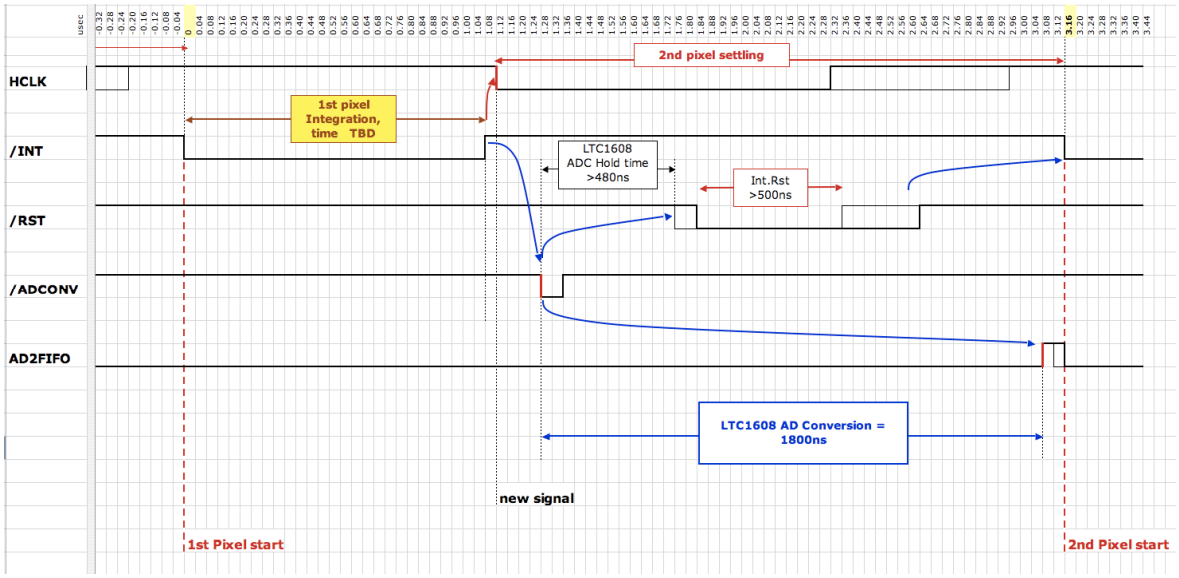

Figure 8. Pixel timing: The video settling begins on the falling edge of HCLK, when the multiplexor's horizontal shift register selects the next column. The integration on the signal is halted just prior to this edge. The ADC's sample and conversion times and Integrator Reset (/RST=low) are hidden within the 2µs settling time of the mux and video chain, so that the time for the integration on the new video level (/INT=low) is maximized.

Figure 8 shows how the control signals have been arranged so that the overheads for signal sampling, conversion and data transmission are overlapped with the signal settling after the falling edge of the Horizontal Clock. This minimizes the overheads so that the time spent integrating on the signal sample can be maximized, which in turn minimizes the impact of the high frequency noise sources. Alternatively, faster pixels allow more sample averaging to beat down the mid to low frequency noise. The data plotted in Figure 9 were acquired to determine empirically what is the optimum allocation of time between signal integration (slower pixels) and coadding (more frequent visits to a given pixel). Noise versus frame rate reaches a broad minimum when settling time is 2 µs and sample integration time is ≥3 µs. We chose 2µs settling and 4µs sample integration time for a 6µs pixel, which is considerably faster than the standard 10µs.

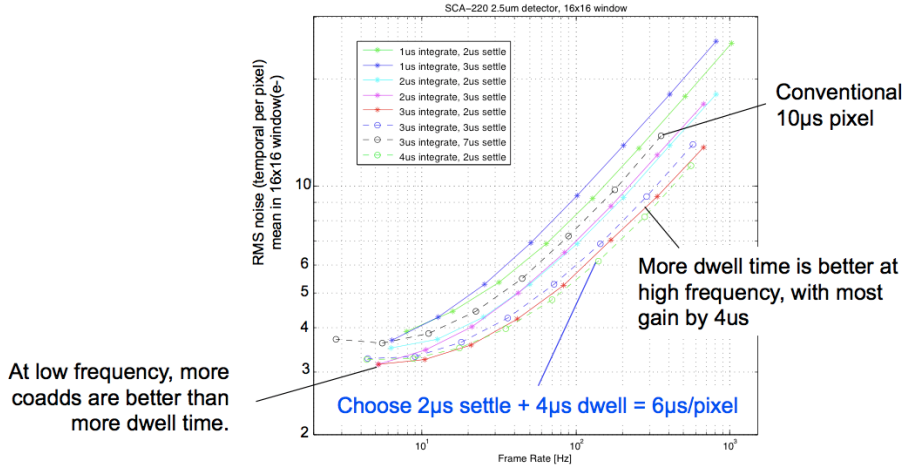

Figure 9. Noise versus frame rate for various combinations of settling and sample-integration time.

4.2 Noise as function of frame rate

The change in the relationship between noise and frame rate as a function of frame size and temperature, shown in Figure 10, allows us to identify a variety of noise sources. The right-most point for each frame size represents a simple CDS readout where each exposure is synthesized by subtracting values in successive frame scans without the benefit of any averaging to reduce noise. The noise is reduced as nearly the half power of the number of coadds made possible at lower frame rates. Smaller (thus faster) windows benefit from more coadds. The curves flatten after about 70 coadds due to 1/f noise whose impact is not reduced by averaging. For temperatures below about 120K, the noise curves turn up at longer frame times because of multiplexor glow (discussed below). Dark current is negligible at these temperatures even in the presence of self-heating (see section 5.2). A clue to the fact that the noise turn-up is due to multiplexor glow is that the noise scales as number of reads and not frame time below 130K. Above this dark current does begin to dominate, but only at low frame rates.

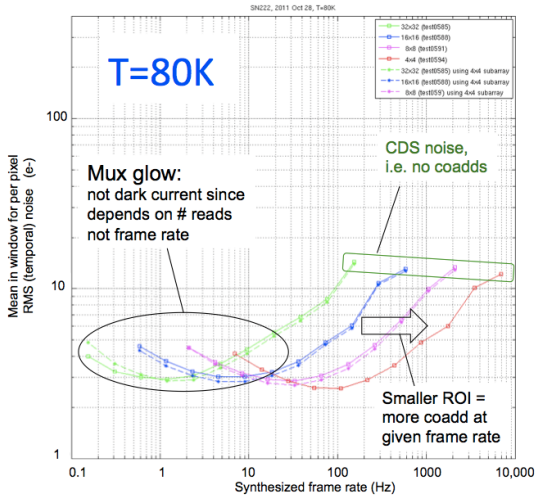

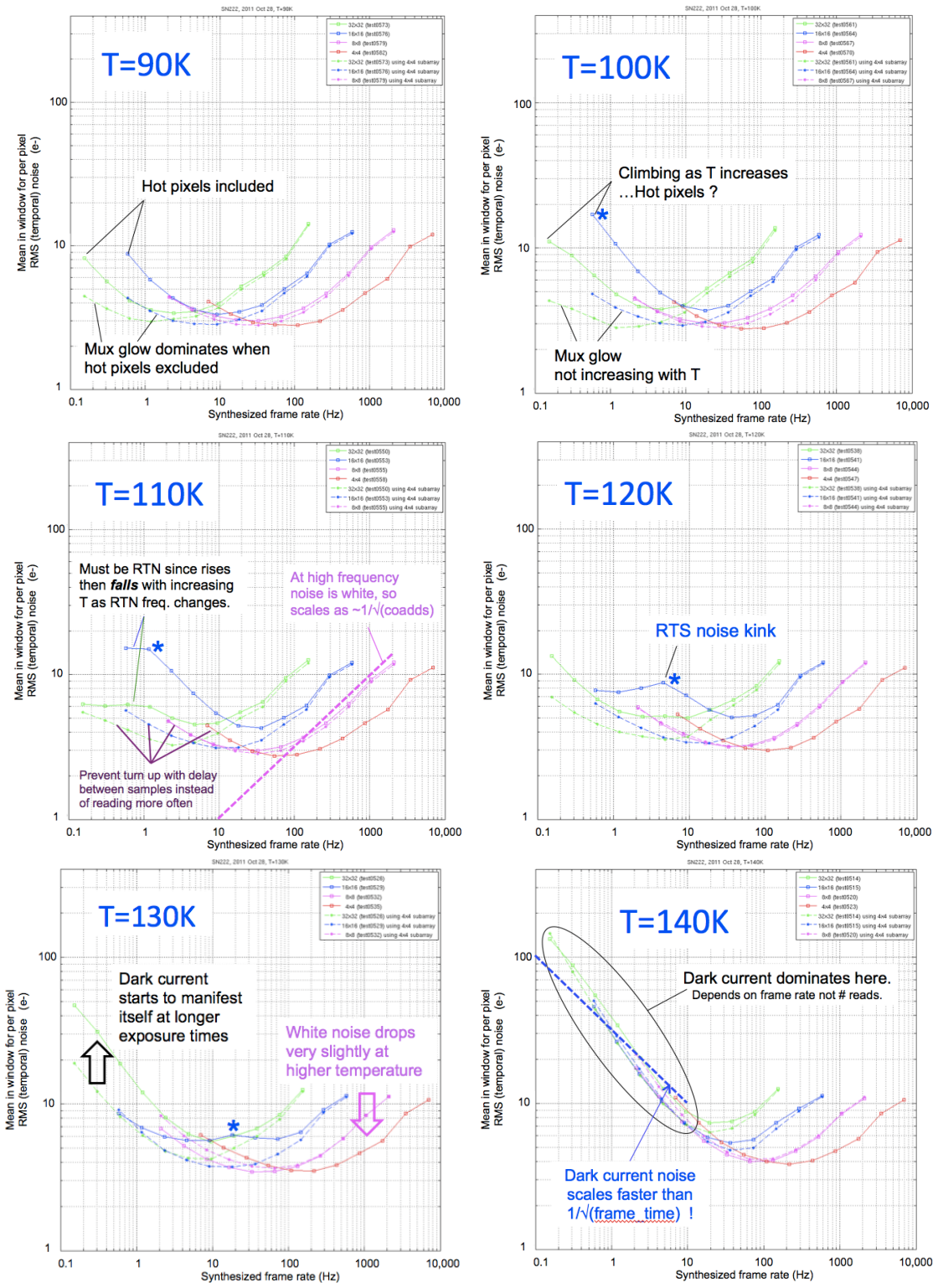

Figure 10. Mean noise versus frame rate for single windows of various sizes. At each temperature and window size, the various frame rates were synthesized from a long sequence of non destructive samples recorded to host RAM and written as a single "film strip" file up to a gigabyte in size and holding hundreds of thousands of frames. The experiment was repeated for 4 window sizes at seven temperatures ranging from 90K to 140K.

4.3 Multiplexor glow

In Figure 11, signal is plotted against time for a rapid sequence of 70,000 frames. Smaller windows are visited more often per unit time and see greater signal slope in the dark. This slope is found to depend on number of visits rather than elapsed time indicating that the predominant source of signal is multiplexor glow and not dark current. An alternative interpretation might be that self heating increases when the power dissipation is concentrated in smaller windows and that the dark current increases for this reason, however dark current induced by self-heating is shown in section 5.2 to be too to exhibit exponential settling with time constant ~0.3 seconds which is much too shorter to account for the linear gradients on 20 to 70 second times scales shown in Figure 11.

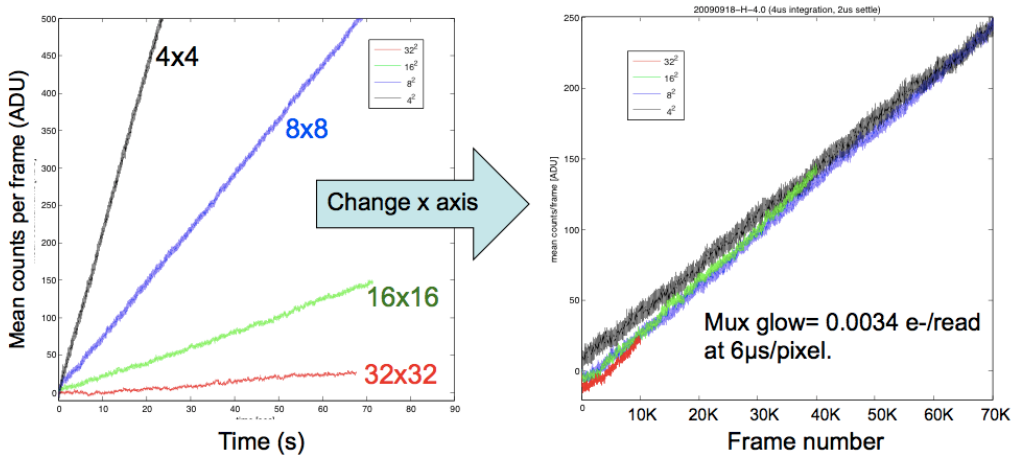

Figure 11. Dark signal is plotted versus time (left) and again versus frame number (right) for a variety of frame sizes.

4.4 Noise model

Plotting noise versus frame rate for individual pixels, as in Figure 12 for example, shows that the shapes of the curves are very similar for all low noise pixels forming the core of the noise distributions seen in Figure 16, the while those lying in the upper tail of the distribution have a very different frame rate and temperature dependence indicating that other mechanisms are in play. Let's first consider a model that fits the well-behaved pixels.

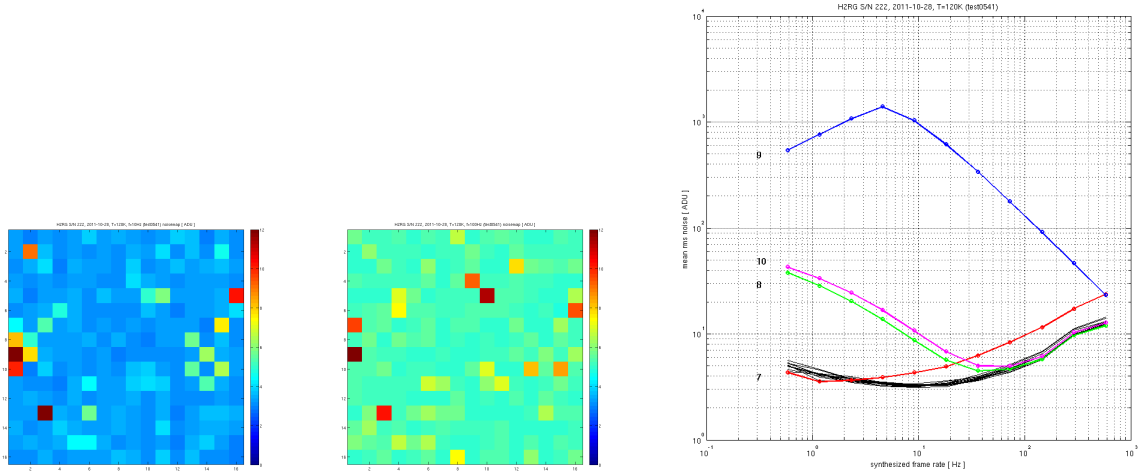

Figure 12. Noise maps at 10Hz (left) and 1kHz (right), as described in section 4.5. Noise is plotted versus frame rate *for individual pixels* in the leftmost column of the noise maps. Note how curves for low noise pixels all have very similar shapes while the four high noise pixels behave very differently. The upper curve (from column 1, row 9) exhibits RTN, while those from rows 8 and 10 may suffer from high dark current. The pixel on row 7 (red curve) has abnormally high white noise.

In Figure 13, measured noise averaged among typical pixels (open symbols) is compared to a model parameterized as the quadrature sum of a white noise component which scales as 12e- CDS noise divided by the square root of the number of coadds, a floor due to 1/f noise, and shot noise due to mux glow equal to 0.016 e-/read, which is considerably higher than the 0.0034 e-/read inferred from the integrated signal in Figure 11. This discrepancy has not been resolved. The only parameter needing adjustment in the model was the noise floor which was set to 2.5, 2.4, 2.3 and 2,2 electrons rms respectively for window of 32x32, 16x16, 8x8, and 4x4 pixels.

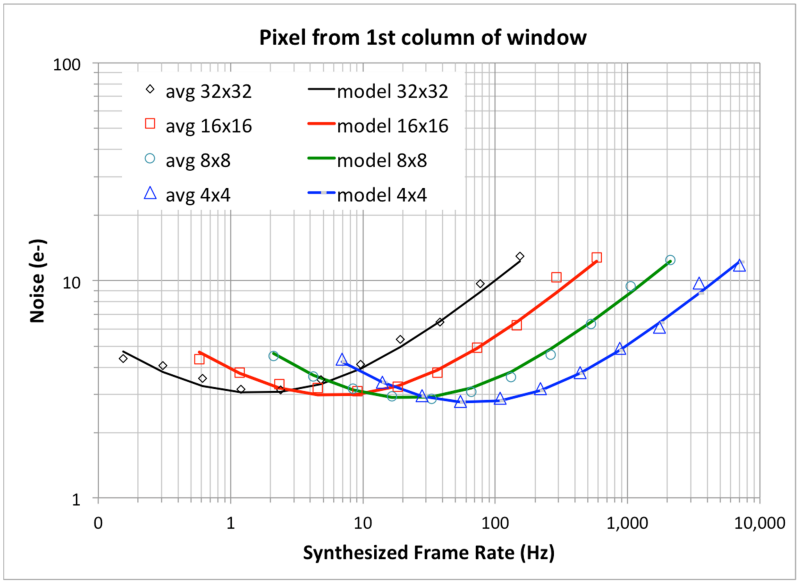

Figure 13. A noise model (solid lines) is compared to measured data (open symbols), averaged over those pixels that show typical behavior. The model consists of the quadrature sum of white noise = 12e-/√coadds, shot noise from mux glow = √(0.016*coadds), and 1/f noise floor adjusted from to 2.5 e- to 2.2 e- for windows from 32x32 to 4x4 respectively.

4.5 Noise Maps

The noise maps shown in Figure 15 were made by computing the standard deviation for each pixel across all exposures at various frame rates synthesized from a single film-strip file using Differential Multi-Accumulate processing with differing coadd factors. A 4x4 pixel window was moved around the full area of the 2048x2048 detector in 256 pixel increments, beginning 128 pixels from the edge, then 4x4 noise maps from each position were packed into single 32x32 images as illustrated in Figure 14.

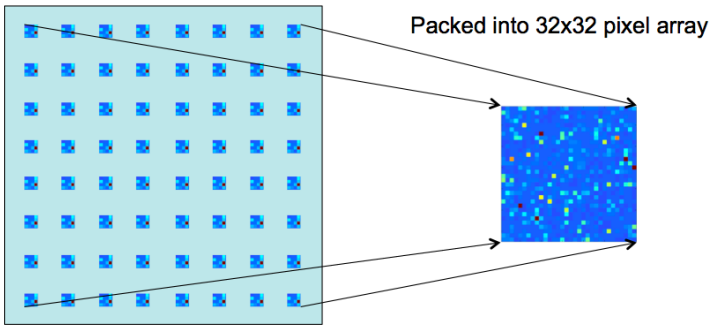

Figure 14. The noise maps shown in Figure 15 were created by combining noise maps for 4x4 windows placed at 256 pixel intervals across the whole detector. Data from 4x4 pixel window was collected separately, then noise maps were computed after synthesizing the various frame rates from the same data sets using the Differential Multi-Accumulate algorithm.

A comparison of the noise maps in Figure 15 reveals that there is very little correlation in the high noise pixels, across temperatures or frame rates. This is a hallmark of Random Telegraph Noise, which is discussed further in section 4.6. It greatly complicates observation planning since the bad pixel maps become a function of exposure time (=1/frame rate). Only at the lowest frame rates (10-100Hz) and highest temperatures tested (130-140K) is dark current a significant

source or noise. In the 140K noise map at 10Hz, the dark current is higher than would be predicted from full frame data. This is due to self-heating (see section 5.2). At 10Hz and 80K to 110K the noise is seen to be higher in the middle of the window than at the edges. These are the cases where noise is dominated by mux glow. It would appear to be lower at the edge of the 4x4 window, as observed, if the glow from and given pixel also illuminates is neighbors.

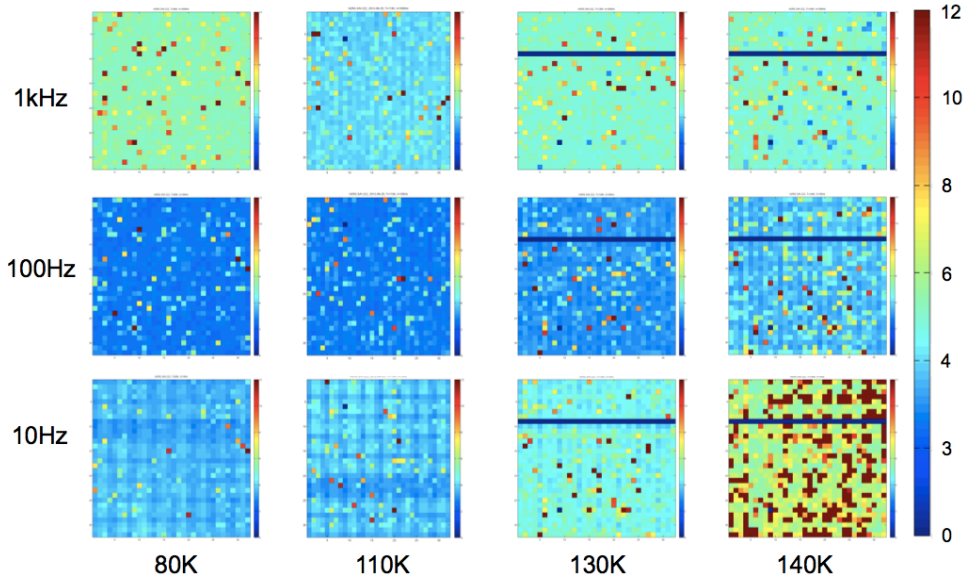

Figure 15. Noise maps (e-) composed from 4x4 windows at 256 pixel spacing over the full detector area, at 10-1000Hz frame rates and 80-140 K. The zero noise row in the 130 K and 140K maps was caused by a mux fault at that location.

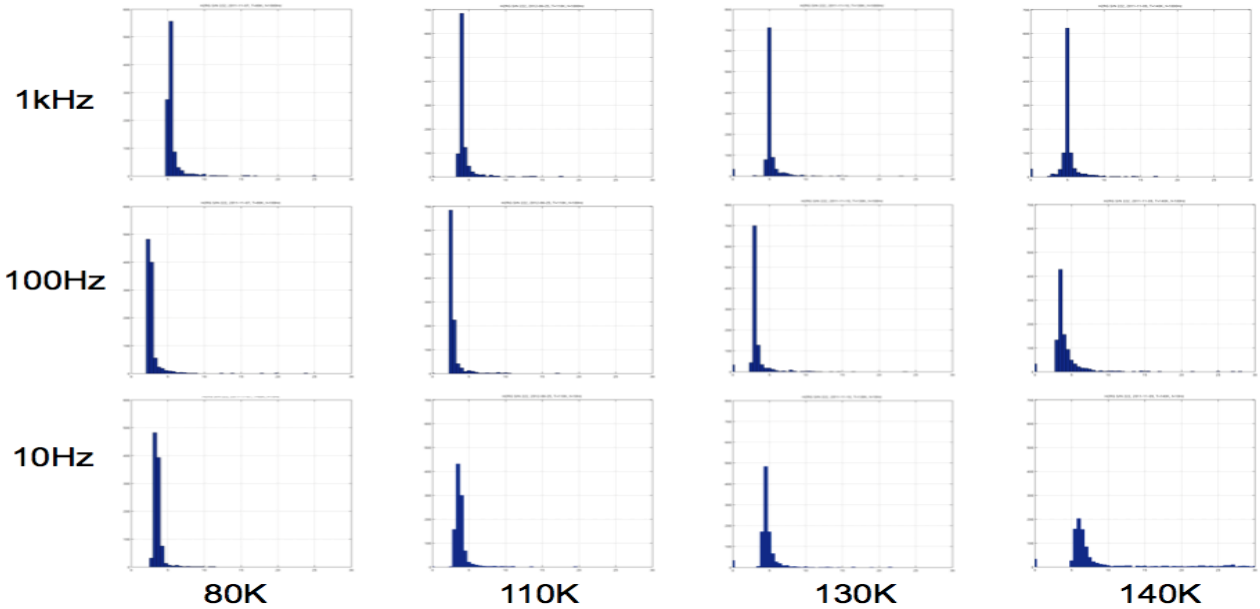

Figure 16. Histograms made from the noise maps in Figure 15. X-axis ranges from zero to 30 e-.

4.6 Random Telegraph Noise

The histograms in Figure 16 indicate that most pixels exhibit similar magnitude and frame rate dependence. These "normal pixels" follow the model presented in section 4.4, but an examination of the high noise pixels reveals a very different frame rate dependence. Except for the very few pixels that exhibit extremely high leakage current, high dark current is not a problem below 130K for the high frame rates used for wavefront sensing. There is however a significant tail in the noise distribution which is created by Random Telegraph Noise (RTN). A single electron trap in the channel

of the pixel buffer MOSFET modulates its transconductance, changing gain and offset markedly between the filled and empty states. The transitions have fixed amplitude and random timing near some characteristic frequency. The capture and release time constant decrease steeply with temperature. This noise mechanism is common in the surface channel MOSFETs typically employed, and far less prevalent in the more esoteric buried channel MOSFETs, since traps are less common in the bulk material than at the oxide interface.

Although most pixels do not suffer from RTN, it is more widespread than commonly believed. The concentration of noise power at certain frequencies can conceal the presence of a trap. When the RTN's characteristic frequency is much *lower* than the frame rate only a small fraction of exposures will be affected by the transitions so the total noise power goes down (and outlier rejection is possible). When the RTN frequency is much *higher* than the coadd time then the RTN averages away quickly. Thus RTN becomes prominent only when it characteristic frequency nears the frame rate. Figure 17 shows how the frequency of the RTN increases rapidly with operating temperature. The tendency for RTN to have strongest effect when the frame rate is similar to the RTN frequency, leads to a high noise "kink" in the curves, marked with a blue asterisk in Figure 10. This noise peak moves to higher frequencies as temperature is increased.

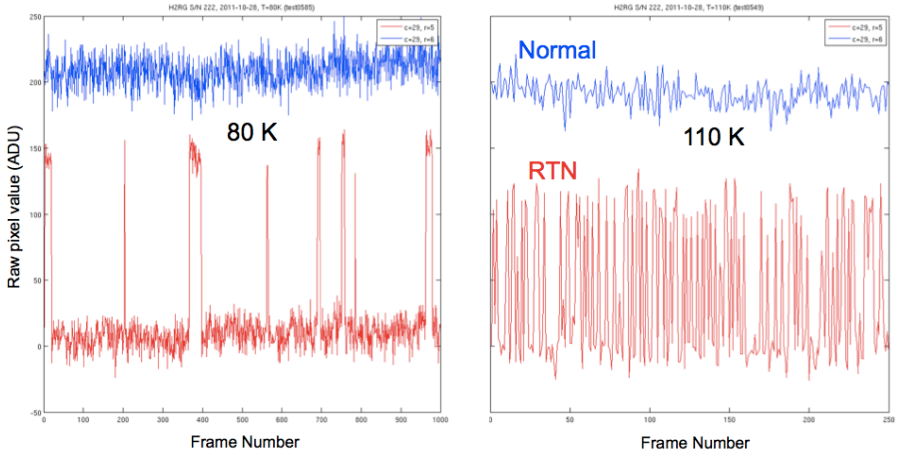

Figure 17. Raw dark signal versus frame number for adjacent pixels at 80 K (left) and the same pixels at 110 K (right). The upper trace shows a quiet pixel. The pixel on the lower trace has similar underlying noise but suffers from RTN due to a single electron trap. Note the steep drop in capture and release times at the higher temperature.

5. OPERATIONAL ISSUES

5.1 Bad pixel mapping

At frame rates higher than 10Hz and with reasonable cooling, it is rare for dark current to be significant even for what might normally be considered "hot pixels". Given that interconnect yield is generally high and leaky pixels are rare, the dominant source of bad pixels is RTN. Since RTN frequencies vary widely from pixel to pixel, the bad pixel map will depend on the frame rate selected. Thus there is no universal bad pixel map but a bad pixel "cube" having frame rate as the third dimension. In addition the RTN's characteristic frequency is highly temperature dependent so this calibration must be done at the operating temperature. These are significant operational complications, which were not appreciated until this study was conducted.

5.2 Self heating

The majority of the power dissipated in the pixel is due to the current through the pixel buffer MOSFET which only flows when the pixel is being addressed. In full frame readout, raster scanning distributes this power over the 64x2048 pixels served by each of the 32 channels. For windowed readout, with coadding as described in this paper, the same power is concentrated in a smaller area. A 4x4 pixel window experiences the same power flow in 8192 times smaller area, so the local temperature rise will be significantly greater.

To illustrate the effect of self-heating, an 8x8 window was read continuously for long enough to establish thermal equilibrium, then the window was expanded to the surrounding 32x32 pixels, and readout was continued without a pause.

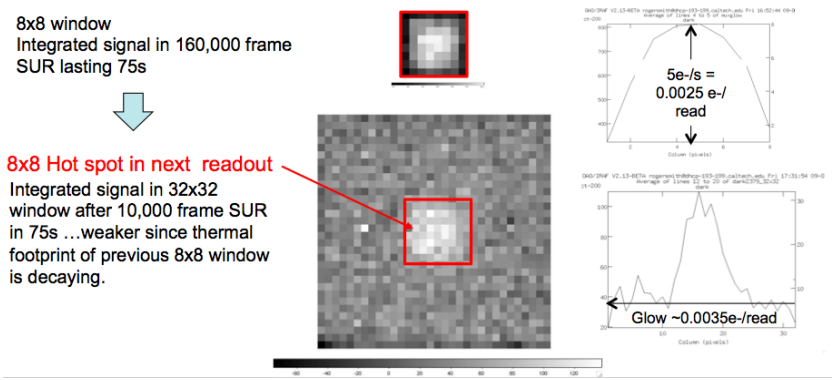

Figure 18. 8x8 window readout showing a profile in the cumulative signal mostly due to mux glow (top). The 32x32 window surrounding it (bottom) was read out immediately afterwards reading the 8x8 window and exhibits both the expected mux glow and elevated dark current at the site of the 8x8 window due to the greater self heating which occurred during the 8x8 window readout.

Dark current increases in response to the self-heating so the acceptable operating temperature should be inferred from noise-versus-frame-rate curves (Figure 10) rather than dark current measurements made with full frame readout. However, the difference turns out to be small and will be most noticeable at higher temperatures.

In addition to increased dark current, self-heating produces a change in video offset due to the dependence of MOSFET threshold on temperature. This video offset is removed by the subtraction of a reference frame only if it remains stable throughout the exposure. A typical cumulative offset change due to self-heating during readout is shown for 4x4 window in Figure 19. Clocking was suppressed during the preceding 30 seconds so that there was no self-heating. The 397e- total offset change implies only 0.5 K change in temperature in the 4x4 window, if the 800e-/K dependence of video offset on H2RG package temperature for full frame readout is used. This is probably an over estimate since the temperature dependence of video offset will be greater when the pixel temperature changes without the compensating effect of the same temperature change in the output buffer at the edge of the package.

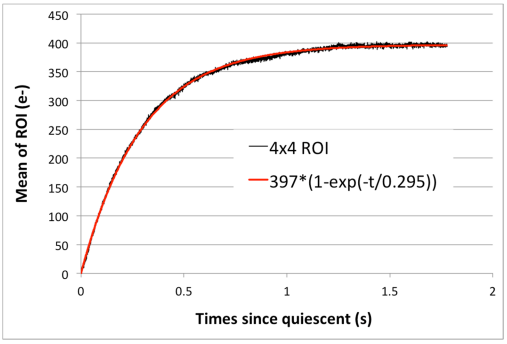

Figure 19: Mean video offset for a 4x4 ROI changes by only 397 electrons due to self heating when reading continuously after 30s with no power dissipation (no pixels addressed, no clocking), and exhibits a dominant time constant of 295ms.

The initial slope is 1345e-/s, implying 13.45 e- in the initial frame at 100Hz synthesized frame rate, or 1.3e- at 1kHz. This transient is suppressed by executing the same clocking pattern during idle so that thermal settling begins before the exposure starts.

5.3 Thermal settling after window move.

The pattern of signal offset induced by self-heating, illustrated in Figure 18 and Figure 19, will shift to realign with the window over a brief period after the window is moved. This is a particular concern when the window is moved by less than its width since the self-heating pattern will skew the background beneath the guide star and produce a significant centroiding error until a new thermal equilibrium is established. Single pixel motions of the window will occur in real time as the AO control system compensates for differential atmospheric refraction which changes the apparent angular

separation of science target and guide star. Figure 20 shows the pattern induced by a two-pixel shift of a window to the left when reading a 4x4 window and coadding to achieve 1 kHz frame rate. Figure 21 shows that the pattern in Figure 20 decays to negligible levels in 6 ms, making this a minor problem.

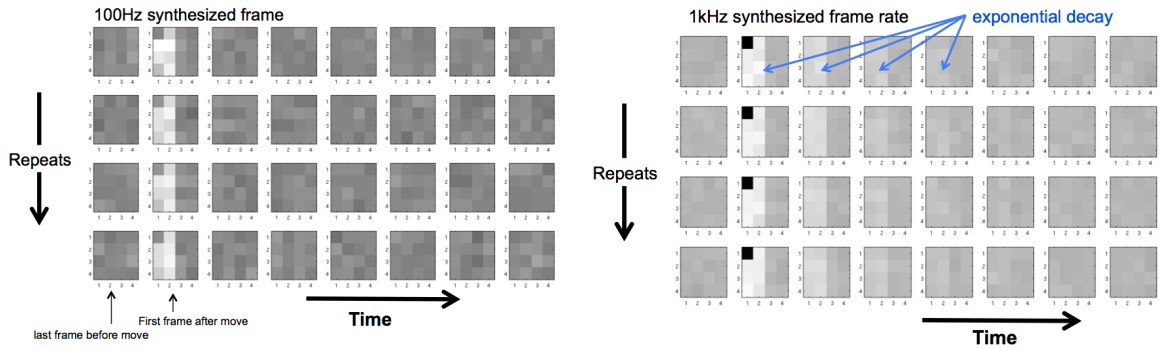

Figure 20. The offset pattern induced by self-heating, when 4x4 window is moved two pixels to the left. The frames are generated using the Differential Multi-Accumulate algorithm, coadding to get 1ms per frame.

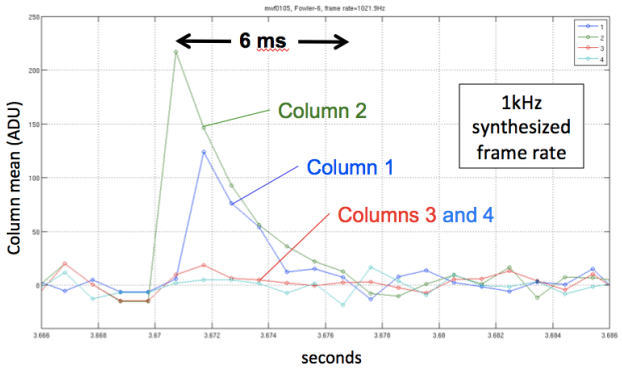

Figure 21. The mean pixel value decays in about 6 ms when 4x4 window is moved two pixels to the left, for Differential Multi-Accumulate algorithm, coadding to synthesize 1 kHz frame rate.

5.4 Window reset ghosts

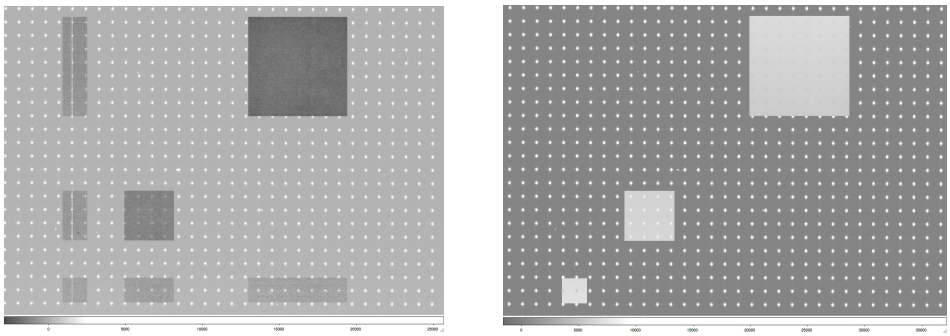

Figure 22. At left, while a uniform grid of spots was projected, several windows (on the diagonal) were reset in turn causing a reset ghost at the intersection of the old columns and the new lines. At right, an extra global reset was inserted with window address pointers set to the edge of the sensor, outside the band of interest, before resetting the target window.

When a window is moved then reset at the new location using global reset mode, not only are the pixels in the target window reset but so too are the pixels having the same column range as the previous window location and the line range corresponding to the new window. This is because the column range is latched and there is a race condition in the multiplexor's reset logic, which enables the reset to begin before the new column range has propagated through the latches. This becomes apparent if a full frame is read out after resetting several windows, as shown in Figure 22. This

could occur in TRICK under rare circumstances where there is a switch from window mode to full frame readout but in practice the effect is erased during the intervening idle. In window mode interference between the reset on one window and its neighbor is rendered benign by resetting all windows before beginning to read any of them. Another remedy, not needed here, is to move the window to line 1, and insert an extra global reset pulse there so that the "reset ghost" is moved to the edge of the sensor, as illustrated in the right panel of Figure 22.

5.5 Column offsets

An offset is observed in columns in which a window is located due to capacitive coupling between the column select lines and the signal sense node. This is only seen when a window is selected in the area being read between the time the reference frame is read out and when the signal frame is read. Since TRICK only updates the window positions at reset, this effect is removed by the subtraction of the new initial frame(s) and remains invisible. The offset can be moved out of the way by changing the window address pointers as shown in Figure 23.

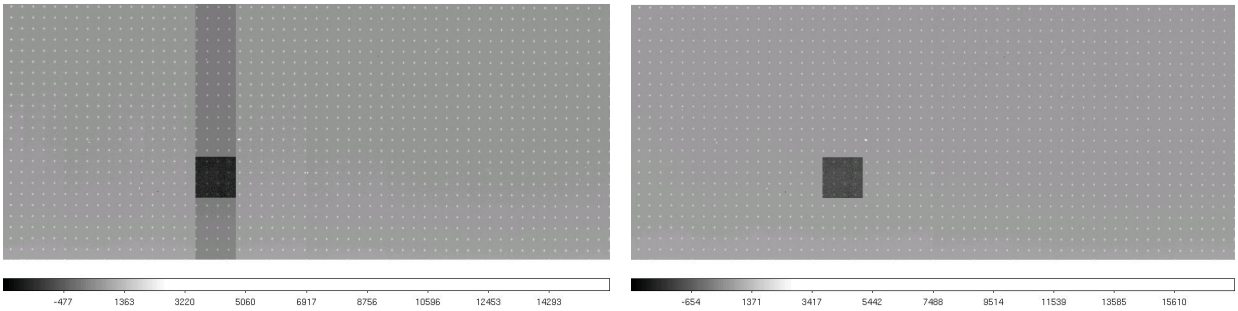

Figure 23. Left: an offset is observed in entire columns when a window is selected within a larger area being read out. In practice this is not a problem since windows are only moved at the time of a reset and so that the offset is subtracted out. Right: the same image is displayed but the column offset has been moved to the edge of the detector by changing the window address pointers.

6. CONCLUSIONS

The differential multi-accumulate readout scheme delivers 3 electron read noise at frame rates up to ~100Hz for small windows and scales as the square root of the number of samples at higher frame rates. Below the frame rate at which 1/f noise dominates (around 100Hz), noise increases due to mux glow, unless longer exposures are created by inserting delays between samples rather than coadding more samples. Above the 1/f noise floor, optimum noise performance is achieved at 6 μs/pixel rather than the typically quoted 10 μs/pixel due to the larger number of samples averaged per unit time. Operating temperature is not critical at any of these frame rates and can be as high as 120K with little noise degradation from hot pixels or self-heating effects. The principal cause of "bad pixels" is not dark current (hot pixels), hybridization failure or low QE, but is Random Telegraph Noise, which creates a sufficient number of much noisier pixels to be a concern. Noise maps change markedly with frame rate (exposure time) and temperature, complicating the planning of observations. Thus a steerable fold mirror, replacing the manually adjusted mirror in TRICK, would be beneficial as it would allow noisy pixels to be avoided without moving the science target.

ACKNOWLEDGEMENTS

This investigation was initially funded by the Thirty Meter Telescope, as part of a larger design study for the On-Instrument Low-Order Wavefront Sensor for the TMT Infrared Imaging Spectrograph. The performance demonstration led to an NSF ATI grant to construct, TRICK, the NIR Tip Tilt sensor for the Keck-1 AO system feeding OSIRIS. This in turn supported continued refinement of the readout algorithm and deeper understanding of the noise processes. This paper has been cleared for public release under the ITAR regulations by the US Department of Defense, Office of Security Review (ref. #4 12 S-2750, Aug 14, 2012).

REFERENCES

[1] http://www.brooks.com/products/vacuum-solutions/waterpump-and-chillers/pcc-compact-coolers
[2] http://www.arscryo.com/MR.html